Field-of-View Calibration of the Microwave Limb Sounder on the Upper Atmosphere Research Satellite

Richard E. Cofield
Jet Propulsion Laboratory
4800 Oak Grove Drive MS 183-701
Pasadena CA 91109-8099. USA
T: 818.354.2501 F: 818.393.5065 EMail: rick@mlsrac.jpl.nasa.gov

Abstract: This paper describes the field-of-view (FOV) calibration of the Microwave Limb Sounder (MLS) on board NASA's Upper Atmosphere Research Satellite (UARS). Calibration data are derived from measurements and analytical models, combined with in-flight data. Particular emphasis is given to pointing calibration and estimation of far sidelobe levels and radiance offsets, using both the Moon and the residual signals when the FOV is pointed high above Earth's atmosphere.

INTRODUCTION

The MLS represents the first implementation of microwave limb sounding from space (Barath, 1993). The MLS senses thermal emission in 6 bands with passive radiometers at 63, 183 and 205 GHz. Its three-mirror antenna system is a 1.6 x 0.8 meter offset Cassegrain matched to diffraction-limited optics and having a surface accuracy of 25 microns. Knowledge of the antenna pattern shape and relative pointing offsets between radiometers is critical for accurate retrievals of temperature, pressure and minor constituent profiles.

A companion presentation (Jarnot, 1994) describes the instrument, its operation, and spectral and radiometric calibration to date, for which the MLS data validation program has indicated absolute accuracy of 5% or better. Complete details of all pre-launch calibrations are in the MLS Calibration Report (Jarnot, 1991).

FIELD-OF-VIEW (FOV) CALIBRATION

FOV calibration consists of the determination of the response of the MLS, as a function of direction, to received power. Table 1 summarizes the antenna subsystem performance, and shows the designations of radiometers (R1-3) and bands (B-6). Dependences of the FOV on scan angle, orbital conditions, and signal frequency within bands, expected to be small compared to its angular dependence, were also characterized for further corrections in the data processing.

The 4π solid angle domain of the FOV functions was divided into two parts based on the rates of change of both the FOV and the atmospheric signal, and on whether we characterize the FOV by model or by measurements. These conform to the partitioning of flight data processing into two "levels":

Level 2: In the solid angle Ω_A, extending ± 0.1 radian $\pm 5°$ about the direction to the nominal center of the scan (limb tangent height $h_T = 30$ km), both the atmospheric signal and the FOV vary rapidly with angle. FOV calibration in this region is performed at Level 2 by a forward radiance model whose inputs include FOV response *vs.* angle from boresight, for each radiometer.

Level 1: Outside Ω_A, the FOV response is $< 10^{-5}$ of its peak value; however, the beam solid angle is so much less than 4π that the average FOV level must be characterized to $10^{-7.5}$. As this was only possible for Band 1 with the available test equipment and far-field range, many of the calibration data depend on analytical models. Since much of this portion of the FOV views radiances which are illatively constant and/or difficult to model (*e.g.* Earth, MLS/UARS structures, and space), calibration is supplied to Level 1 as quasi-constant transmissions and radiance offsets.

LEVEL 1 ANTENNA TRANSMISSION AND RADIANCE OFFSET

The radiance from the antenna which is incident on the radiometer limb port, for channel i in radiometer r, is given by:

$$\begin{aligned} \dot{I}_i^A = {} & \rho_r^P \rho_r^S \rho_r^T \eta_r^{AA} \eta_r^P \dot{I}_i^L \\ & + \rho_r^P \rho_r^S \rho_r^T (1 - \eta_r^{AA}) \eta_r^P \dot{I}_r^{SL} + (1 - \rho_r^P) \rho_r^S \rho_r^T \eta_r^P \dot{I}_r^{OP} \\ & + \rho_r^S \rho_r^T (\eta_r^S - \eta_r^P) \dot{I}_r^{SP} + (1 - \rho_r^S) \rho_r^T \eta_r^S \dot{I}_r^{OS} \\ & + \rho_r^T (\eta_r^T - \eta_r^S) \dot{I}_r^{SS} + (1 - \rho_r^T) \eta_r^T \dot{I}_r^{OT} \\ & - (1 - \eta_r^T) \dot{I}_r^{ST} \end{aligned} \qquad (1)$$

where
- ρ_r^k = Reflectivity of reflector $k = P, S, T$ (Primary, Secondary, Tertiary)
- η_r^{AA} = Beam efficiency of the antenna system: the product of scattering (η_r^{AS}) and diffraction (η_r^{AD}) from the primary aperture plane
- η_r^{Sk} = Spillover efficiency of reflector k with measured feed pattern r
- $\dot{I}_i^L$ = Limb Radiance, channel i
- $\dot{I}_r^{SL}$ = Radiance from outside FOV measurement angle Ω_A, in the limb hemisphere
- $\dot{I}_r^{Sk}$ = Radiance illuminating spillover solid angle for reflector k
- $\dot{I}_r^{Ok}$ = Temperature of reflector k

Equation 1 can be derived by projecting all apertures to the limb port plane, noting through which reflectors and into which spillover each solid angle terminates.

A simplified form of this equation is inverted in Level I calculation of calibrated radiances:

$$\dot{I}_i^L = \frac{1}{\eta_r^A \rho_r^A} \left(\dot{I}_i^A - (1 - \rho_r^A) \dot{I}_r^{OA} - (1 - \eta_r^A) \rho_r^A \dot{I}_r^{SA} \right), \qquad (2)$$

For this simplification, reflectivities $\rho_r^{P,S,T}$ are combined into a single ohmic transmission ρ_r^A, and internal spillover losses similarly with scattering and diffraction losses into the antenna transmission η_R^A. Likewise, the radiances and physical temperatures in equation 1 are combined into *effective* radiances $\dot{I}_r^{OA}$ and $\dot{I}_r^{SA}$.

Transmissions and radiances were combined over all loss mechanisms and antenna components independently for each radiometer. The calculation of $\eta_r^A, \rho_r^A, \dot{I}_r^{OA}$ and $\dot{I}_r^{SA}$ from the measured ρ_r^k and η_r^{Sk}, modelled η_r^{AD}, and for reasonable pre-launch estimates of $\dot{I}_r^{SL}$, $\dot{I}_r^{Sk}$ and $\dot{I}_r^{Ok}$ is discussed in (Jarnot, 1991)

Table 1: MLS Antenna FOV Performance from Ground Calibration and Analytical Models. Knowledge values are 3σ

Parameter	R1,B1 63 GHz	R2,B2-4 205 GHz	R3,B5-6 183 GHz
Half-Power Beam Width (HPBW) (vert.) / °	0.206	0.064	0.077
Knowledge	0.002	0.001	0.001
HPBW (1101.) / °	0.43	0.145	0.152
Knowledge	0.008	0.003	0.002
Beam Efficiency	0.91	0.9	0.91
Knowledge	0.01		
Polarization (angle between of E and vertical at 30 km tangent point) / °	14.	91.	2
Peak cross-polarization / dB	-30	-19	-20
FOV direction (dFOV) knowledge (Wt.) / °			
absolute, B1 to optical reference cube	0.0036		
relative to B1		0.0016	0.0021

Contributors to Level 1 FOV Budget

Four mechanisms contribute to antenna transmission and radiance offsets:

1. Ohmic loss within the antenna reflectors, which was inferred from reflectivity measurements in all bands. Using calculated reflectivities of a silver plate standard, the wo[st-case reflectivity (205 GHz, Primary Reflector) was $R_{1,R2} = 0.9956$ with standard deviation of 0.0008, Combining this error with the systematic uncertainty in the calculation of absolute reflectivity, and the time-k,aryill, g reflector temperatures, gives ohmic efficiencies ρ_r^A ranging from 0.99230.003 in B1 to 0.98930.004 in B2-4.

2. Spillover at antenna reflectors and radiometer apertures. This was obtained by integrating measured feed patterns to the three port edges and to the projected outlines of the antenna reflectors. Uncertainty in normalizing power dominates errors in the limb port baffle transmissions appearing in radiometeric calibration, but tends to cancel in the spillover contribution to η_r^A

3. Scattering by antenna surface irregularities, which was estimated using the contour measurements made during the manufacture of the reflectors, on both coarse (2-D) and fine (1-D) grids. The first dataset was used to calculate errors of form. Fourier analysis of tile second provided correlation length and rms deviation (Marx, 1990) for estimating, *via* the Ruze statistical model (Ruze, 1966), the scattered power which was hidden from FOV patterns with noise floor encountered on the far-field range. This *fraction* of the scattered power was budgeted as antenna transmission. Variations in transmitter power and atmospheric attenuation on the f:ill-field range make this fraction not monotonic in frequency.

   Mean values of the first 3 or 4 sidelobes measured for B2 4 matched the predicted scattered pattern envelope. Model errors of 10% uncertainty in the rms amplitude ϵ and 15% in the correlation length L give 40% uncertainty in fractional scattered power $1 - \eta_r^{AS}$, corresponding to 0.7 K in radiance offset for the worst case, B5-6. "

4. Edge diffraction, for which a model was developed by applying the Geometrical Theory of Diffraction (GTD) to the Primary Reflector leading edge (the limiting aperture at -15 dB taper). GTD patterns match the FOV shape predicted by the aperture-field method and seen in the measured FOVs at ±0.6° for Band 1, where spillover is greatest and this diffraction is most pronounced. Edge diffraction efficiencies η_r^{ed}) appearing in equation 1 ranged from 0.9773 0.009 in B1 to 0.9984 0.001 in 112-4.

Table 2: Antenna Transmission and Radiation Offsets for each MLS Radiometer

Contributor	B1	B2-B4	B5-B6
ρ_r^A (reflectivity)	0.9923	0.989	0.992
scattering	0.999	0.993	0.988
edge diffraction	0.977	0.998	0.992
Primary spillover	0.954	0.985	0,940
η_r^A	0.931	0.976	0.921
T_r^{SA}	144.4 K	243.1 K	118.8 K
T_r^{OA}	252.3 K	256.2 K	251.3 K
range in orbit)		[203,313] K	
Ohmic	1.9 K	2.8 K	2.0 K
Diffraction/Scattering	9.9 K	5.8 K	9.3 K
Total Offset	11.8 K	8.6 K	11.3 K

Table 2 summarizes Level 1 FOV parameters from ground calibration.

FOV CHARACTERIZATION

FOV pattern measurements were performed using frequency-locked transmitters as the signal sources, and were digitally recorded on ground support equipment computers in spherical polar coordinates. Feed patterns were measured in both subassembly and radiometer configurations to verify proper antenna illumination, alignment sensitivity and aperture spillover levels.

Secondary FOV Measurement

FOV patterns of the MLS sensor were characterized at 10 scan angles and ~5 frequencies within each band. Patterns were measured at cuts spaced in azimuth by 22.5°, but at closer spacing near features of special interest and to verify predictions of the analytical models. Polar angle resolution varied from 0.01° in the far sidelobes to HPBW/70 on the main lobe. The ensuing random errors combined with systematic due to range equipment, transmitted power drift and varying temperature fields and gravity loads on the MLS, to give < 3.5% errors in HPBW.

Boresight directions (dFOV) at 63 and 205 GHz were measured to 15 arcsec accuracy, relative to a sensor alignment cube, using a theodolite in conjunction with the RF patterns. A more stringent ? arcsec knowledge of relative dFOV coincidence between radiometers was measured with near-simultaneous patterns using two transmitters.

Figure 1 shows a measured pattern of Band 4 in the limb vertical plane. Noise floors for the 2 polarizations represent the 3km and 1km far-field ranges used. Since the limb radiance variation is significant only in the vertical direction over the ±0.6° domain treated by Level 2, measured FOVS were *collapsed*, i.e. integrated along

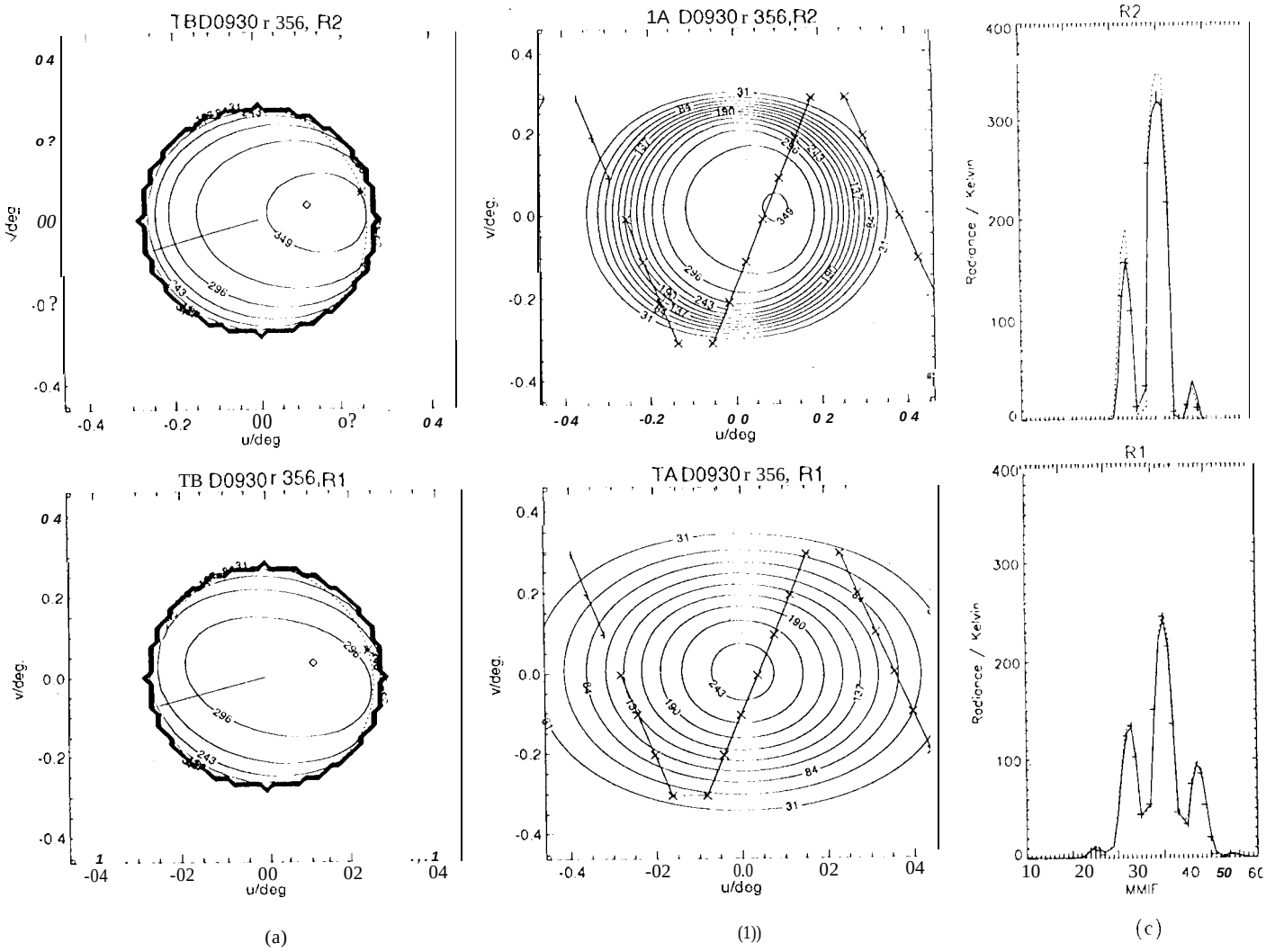

Figure 2: Example of FOV scan through Moon: (a) Model radiance incident on far-field sphere of antenna, showing polarization) dependence and model angular resolution; (b) Convolved limb radiance with scan pattern; (c) Radiance time series before and after iterative solution for dFOV and model gain

attributed to incomplete characterization of the R3 feed patterns and to launch shift. After 2½ years of operation, no instabilities or drifts have been traced to FOV calibration.

ACKNOWLEDGEMENTS

Thanks to Drs. J.W. Waters, H.M. Pickett and M.A. Frerking for providing FOV requirements and guidance in the MLS optics design. Drs. R. F. Jarnot, G. E. Peckham and R. S. Suttie assisted in the formulation of Level1 calibration data. Dr. T. H. Siegel measured the sub-assembly feed patterns. In the antenna's mechanical design, the assistance of Dr. G.J. Klose in fabrication and tolerancing and of Mr. T. O'Toole for thermal deformation analysis was invaluable. For FOV measurements, we thank Mr J.C. Hardy for test range setup, Dr. D. A. Flower and Messrs. C. Colby, E. Fuller and D. Orozco for operation on the range, and E. Poyotena for determination of FOV direction. This work was performed by the Jet Propulsion Laboratory, California Institute of Technology, under contract with the National Aeronautics and Space Administration.

REFERENCES

Barath, F.T. *et.al.* "The Upper Atmosphere Research Satllite Microwave Limb Sounder Instrument, *Journal of Geophysical Research* vol. 98, no. D6 (1990): pp. 1(1,751- 10,762.

Jarnot, R.F. and Cofield, R.E. "Microwave Limb Sounder (MLS) Instrument Calibration Report," Tech. Rep. D-9393 Version 1.0, .11'1/, 1991

Jarnot, R.F. "Calibration of the Microwave Limb Sounder Instrument on the Upper Atmosphere Research Satellite," in International Geoscience and Remote Sensing Symposium Digest, 1994.

Keihm, S.J. "A lunar microwave model for the COBE DMR experiment," 1983. JPL Internal Memo.

Marx, E. and Vorburger, T. "Direct and inverse problems for light scattered by rough surfaces," *Applied Optics*, vol. 29 (1990): pp. 3613 3626.

Ruze, J. "Antenna tolerance theory- a review," *Proceedings of the IEEE*, vol. 54 (1966): pp. 633 640.

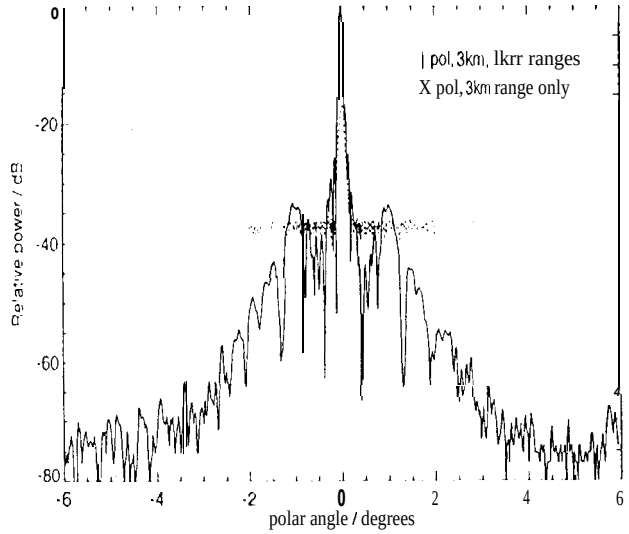

Figure 1: Band 4 Limb Vertical FOV pattern

the horizontal direction, to provide 1-dimensional FOV functions for the forward model.

Dependences of FOV on scan angle and frequency within the band are consistent with known measurement errors and within the requirements of flight data processing algorithms.

For the large (> 100 I{) signals in Bands 1 and 4- 6, variations with scan angle and IF meet the 0.5% functional requirement when convolved with canonical atmospheric radiance kernels at band centers, and compared as differential antenna radiances, ΔT_A. For the ClO signal (Bands 2 and 3), the scatter in the ΔT_A curves is interpreted as the peak to peak excursion of a *random* error whose standard deviation $\sigma \sim$ (l~eak-to-peak)/fi < 0.05 K.

REFINEMENT OF FOV CA LIBRATION FROM IN-ORBIT DATA

Absolute Knowledge of dFOV

soou after launch, MLS pointing was validated at Level 2 by comparing measured radiance spectra growths *vs.* tangent hr-i.gilt, inferred from dead- reckoned pointing, to the forward model. A large offset of 0.12", attributed to launch shift or placement uncertainty between MLS and UARS alignment cubes, was found and corrected in the calibration data

High-Altitude Radiances and 5-20° Roll Maneuvers

Another early refinement to pre-launch FOV calibration was adjustment of scene radiances in equation 1 to make band-averaged radiances at the Ilighest-altitude minor frame (MMIF) match the Planck function values for space radiance. Most of this adjustment occurred in the assumed brightness temperature of UARS seen by MLS Primary spill over. Reductions in total offset radiance ranged from 3.2 to 5.7K. This was validated by radiance data during special scans to the antenna home position (h_T > 250 km) and during $\sim$ 1 orbit of observation with UARS rolled 5° and 20° above the nominal attitude.

Comparison of 1{2 and R3 Retrieved 0_3 Profiles

Ozone profiles retrieved using pre-launch calibration data for R3 exceeded those for R2 by as much as 15%. Both sideband ratio and antenna transmission were adjusted to reduce this discrepancy to < 5%. For the latter, the pre-launch values of R3 baffle transmissions, and the concomitant reflector spillover losses, were replaced by those of R2. Also, an overly conservative estimate of -42dB for the noise floor of FOV patterns was replaced by -50dB. *I.E.*, more information lay in the pre-launch FOV than had been previously budgeted; hence η_{183}^{AA} could be increased accordingly. Further steps to reconcile R2 and R3 ozone treated deviations from pre-launch values of dFOV coincidence

Table 3: Coincidence of Vertical dFOV between Radiometers

	R2- R1 / °		R3- R2 / °	
	$d\epsilon$	3σ	$d\epsilon$	3σ
Pre-Launch	-0.006	0.0016	-0.007	0.0026
from Moon scans	-10008	0.009	-10.004	0.007

Estimation of dFOV Coincidence from Moon in FOV

The envelope of FOV over the available MLS scan range intercepts the Moon approximately 17 clays per year. On four days the MLS scan pattern was altered for $\sim 1/4$ of each of 612 orbits per day, to let the Moon drift through the FOV at controlled scan angles well above the atmosphere. Calibrated radiances were compared to radiances from a lunar microwave model (Keihm, 1983) and convolved with the measured FOVs and with a step function which models **smear'illg** in azimuth due to the integration time. One can relate measured radiances to the model map and its gradient by two pointing angles and a model scaling factor (this scaling error mimics uncertainty in the 10V gain, but is bounded by the uncertainty in high-altitude radiances). These 3 parameters are estimated by minimizing the squared residual sum for the 30 or so MMIFs in each Moon crossing.

Figure 2 shows model radiance maps before and after convolution. The special scan pattern shown was tailored to minimize the a *priori* variance of retrieved vertical pointing, given uncertainty in UARS ephemeris predictions and the unavoidable horizontal drift due to orbital motion. The rightmost panels superimpose measured radiances on model values before and after the retrieval, showing the high signal-to-noise ratio of this technique.

Line 2 of Table 3 results from pooling dFOV between radiometers over all scans to date. Some systematic errors cancel in the subtraction of retrieved angles to obtain the dFOV between R1 and the other two radiometers. Uncertainties for the in-orbit method currently remain several times those claimed for the ground calibration. The change in dFOV between R2 aod R3 is statistically significant and agrees to 0.003° with the offset required to account for the discrepancy between R2 and R3 ozone retrievals. This change is attributed to launch shift and has been used to update data processing software. The scale factor retrieved for 63 GHz differs from 1 by an amount consistent with the Moon model's accuracy at 90 GHz (Keihm, 1983), but the larger deviations for R2 aud R3 may suggest some residual error in far sidelobe level of the FOV functions. This and characterization of model uncertainties are 00W under investigation.

CONC1,[JS1ONS

All FOV characterization eventually required by the software for flight data processing was identified early in the instrument's development, aud nearly all was provided by ground calibration. Exceptions were absolute pointing error, due to launch shift between MLS aud UARS references, aod radiance offset, due to incomplete knowledge of background stray radiance. The latter is spectrally flat aud therefore negligible in Level 2 processing. Subsequent in-orbit refinements have addressed 1{1-1{3 ozone differences, aud are